Neutron capture reactions near the $N = 82$ shell-closure

Saumi Dutta,[*] Dipti Chakraborty,[†] G. Gangopadhyay,[‡] and Abhijit Bhattacharyya[§]
Department of Physics, University of Calcutta 92, Acharya Prafulla Chandra Road, Kolkata-700 009, India
(Received 1 September 2015; revised manuscript received 28 November 2015; published 2 February 2016)

Neutron capture cross sections have been calculated in nuclei near the $N = 82$ neutron shell-closure. These nuclei are of astrophysical interest, participating in the s-process and the p-process. A semimicroscopic optical model has been used with the potential being obtained through folding the target density with the DDM3Y nucleon-nucleon interaction. Theoretical density values have been calculated using the relativistic mean-field approach. The calculated cross sections, as a function of neutron energy, agree reasonably well with experimental measurements. Maxwellian-averaged cross sections, important for astrophysical processes, have been calculated.

DOI: 10.1103/PhysRevC.93.024602

I. INTRODUCTION

After the seminal work of Burbidge *et al.* [1], the method of creation of heavy elements through the slow neutron capture or s-process has been firmly established. A recent review that discusses our current understanding of the s-process may be found in Käppeler *et al.* [2]. It is now understood that a major fraction of the nuclear abundance in the mass region $90 < A < 209$ is due to the main s-process that takes place in He shells in low-mass asymptotic giant branch stars of moderate mass.

The role of the neutron capture reaction in the s-process has been explored in many works. More accurate measurements have shown the inadequacy of the classical site-independent s-process and have paved the way to coupling with stellar models. A mass region, where the reaction cross section plays a very important role, lies near the $N = 82$ shell-closure. Here, the elements Cs ($Z = 55$) to Sm ($Z = 62$) have small cross sections for neutron capture reactions because of the proximity of the shell closure. Hence, they act as bottlenecks for the s-process reaction path. An s-process peak occurs at ^{138}Ba. There are several s-only nuclides such as ^{134,136}Ba, ^{142}Nd, and ^{148,150}Sm in this mass region. In the case of pairs of s-only isotopes such as ^{134,136}Ba, the cross sections and the abundances can be used to obtain the branching ratios of the s-process. Nuclei on the s-process path that have comparable β-decay rates and neutron capture rates act as branch points as the nucleosynthesis path bifurcates towards both the proton- and neutron-rich sides while passing through them. The cross sections at the branch points and s-only isotopes can provide important clues to the physical environments where the s-process takes place.

Although experimental measurements are available for many isotopes in the mass region, cross-section values are required for some unstable nuclei those are important in determining the branching ratios. Such nuclei include ^{134,135}Cs, ^{141}Ce, ^{147}Nd, and ^{147,148}Pm. We should also remember that although the classical or canonical s-process calculations use the Maxwellian-averaged cross sections (MACS) at a single thermal energy (≈30 keV usually), recent approaches, which couple stellar models with the s-process network, need MACS values at different thermal energies. Measurements are not always available and extrapolation to too distant values from the measured ones may lead to errors. Theoretical calculations can supplement the experimental measurements in this regard.

There are some neutron capture reactions in this mass region whose studies are relevant for the astrophysical p-process. Photodissociation reactions such as (γ,n) reactions occur in extremely hot environments. Explosively burning Ne/O layer in core-collapse supernovae heated by the outgoing shock wave may provide such an environment. Cross-section values are very important as various photodissociation reactions such as (γ,n), (γ,p), and (γ,α) compete at high temperatures. The emitted neutrons may also be absorbed after the shock wave passes through the layer. Thus it is very important to measure the cross sections for relevant (γ,n) reactions at thermal energies. The reverse process, i.e., (n,γ) reactions, may serve the purpose. For example, Dillmann *et al.* [3] studied a number of (n,γ) reactions with neutrons from the ^{7}Li$(p,n)^{7}$Be reaction to simulate a Maxwellian neutron distribution at 25 keV thermal energy.

In the study of the s-process the energy range of the neutron as a projectile is low enough so that one has to deal with the radiative thermal neutron capture cross section. Thus in the present study we calculate the σ_γ cross section in which the target after absorbing the neutron emits one or more γ rays. Thus, our interest in this work lies in the radiative neutron capture, i.e., (n,γ) reactions. The study includes direct capture cross sections by excited states also, though contribution of direct capture cross-sections is small in the energy region of our interest. Radiative neutron capture reactions have been studied in various methods. Older experiments usually used neutron beams of comparatively wide resolution. As the resonances in this region are narrow (less than 1 eV), one gets an average cross section in such experiments. Extremely high-resolution experiments using the neutron time-of-flight technique (TOF) have been used to study the resonances. However, we are more interested in the MACS. In such cases, the data have been compressed into coarse energy bins to obtain MACS values. In some other experiments, sources of neutrons have been used that closely simulated the thermal neutron spectrum at certain

[*]saumidutta89@gmail.com
[†]diptichakraborty2009@gmail.com
[‡]ggphy@caluniv.ac.in
[§]abhattacharyyacu@gmail.com

TABLE I. Parameter set for the FSU Gold Lagrangian density. The parameter κ and meson masses m_s, m_v, and m_ρ are in units of MeV.

m_s	m_v	m_ρ	g_s^2	g_v^2	g_ρ^2	κ	λ	ζ	Λ_v
491.500	782.500	763.000	112.1996	204.5469	138.4701	1.4203	+0.023762	0.06	0.030

temperatures. They can provide direct measurement of MACS values.

In the present work, we have studied low-energy neutron capture cross sections of the nuclei near $N = 82$. In the next section, we briefly present our formalism. In Sec. III, we discuss our results for important neutron capture reactions near $N = 82$ shell-closure, at various neutron energies, and compare them with experimental measurements. It is then followed by calculation of the MACS values, first at 30 keV and later at different thermal energies for some selected isotopes. Finally we summarize our work.

II. CALCULATION

A. Relativistic mean-field calculation

In relativistic mean-field (RMF) theory nucleons are treated as point particles interacting via the exchange of mesons and photons. In the present work, we have chosen the Lagrangian density FSU Gold [4], which contains self-interactions for the isoscalar-scalar sigma meson (ϕ) and the isoscalar-vector omega meson (V) as well as interaction between the isovector-vector rho meson (b) and omega meson. The interaction part has the usual form,

$$\mathcal{L}_{\text{int}} = \bar{\psi}\left[g_s\phi - \left(g_v V_\mu + \frac{g_\rho}{2}\tau b_\mu + \frac{e}{2}(1+\tau_3)A_\mu\right)\gamma^\mu\right]\psi - \frac{\kappa}{3!}(g_s\phi)^3 - \frac{\lambda}{4!}(g_s\phi)^4 + \frac{\zeta}{4!}\left(g_v^2 V_\mu V^\mu\right)^2 + \Lambda_v\left(g_\rho^2\mathbf{b}_\mu\cdot\mathbf{b}^\mu\right)\left(g_v^2 V_\mu V^\mu\right). \quad (1)$$

The nucleon and the photon fields are represented by the wave functions ψ and A, respectively. The meson masses and the coupling parameters are given in Table I.

The Klein-Gordon equations for meson fields and Dirac equations for baryon fields are obtained as the usual Lagrange's equations. Pairing is incorporated in the continuum BCS approximation using a delta pairing potential $V(\mathbf{r_1},\mathbf{r_2}) = -V_0\delta(\mathbf{r_1}-\mathbf{r_2})$. The pairing strength V_0 has been chosen to be 300 MeV for both protons and neutrons. The equations are solved in co-ordinate space using spherical approximation. The equations are solved by iterative technique in a grid size of 0.1 fm. The Dirac equations are solved using a fourth order Runge-Kutta method by integrating inwards from large r as well as outwards from small r and the energy eigenvalues are varied to make the wave function continuous at some appropriate matching radius. The meson fields are solved by integrating over the appropriate Green's function using Simpson's rule. The iterations are repeated till the desired accuracy is achieved.

B. Folding model analysis and potential formation

We have used a semimicroscopic procedure to calculate the neutron capture cross sections in the present work. This method has been followed in a number of our recent works [5–10]. For example, in Chakraborty *et al.* [10], this procedure has been utilized to study proton capture reactions, important for the astrophysical p-process in the mass 110–125 region. In the present approach, we extend it to study neutron capture reactions near the $N = 82$ shell-closure.

To briefly describe our procedure, we have assumed spherical symmetry for the target nuclei. The density profiles of the nuclei have been calculated in coordinate space in the RMF approach as mentioned earlier. The charge density (ρ_{ch}) is obtained from the point proton density (ρ_p) using a standard Gaussian form factor, $F(r)$ [11], as follows:

$$\rho_{\text{ch}}(\mathbf{r}) = e\int \rho_p(\mathbf{r}\prime)F(\mathbf{r}-\mathbf{r}\prime)d\mathbf{r}\prime, \quad (2)$$

$$F(r) = (a\sqrt{\pi})^{-3}\exp(-r^2/a^2), \quad (3)$$

with $a = \sqrt{2/3}a_p$, where $a_p = 0.80$ fm is the root-mean-square (rms) charge radius of the proton. The charge density thus obtained is used to calculate rms charge radii for some nuclei in and around the concerned region of shell closure to compare with experimentally available values. Comparison with measured values serves as a check on the applicability and reliability of the Lagrangian density used in the calculations. Charge density has been chosen for comparison because its experimental measurements are available from electron scattering.

The nuclear density (sum of the point proton density and the point neutron density) has then been folded with the DDM3Y nucleon-nucleon interaction to obtain the optical model potential. The interaction at distance r for density ρ and the projectile energy in the center-of-mass frame E, supplemented by a zero-range pseudopotential, is given by

$$v(r,\rho,E) = t^{\text{M3Y}}(r,E)g(\rho), \quad (4)$$

with the M3Y interaction [12,13] in MeV,

$$t^{\text{M3Y}} = 7999\frac{e^{-4r}}{4r} - 2134\frac{e^{-2.5r}}{2.5r} - 276\left(1-\frac{E}{200A}\right)\delta(r). \quad (5)$$

Here E is given in MeV, r is in fm, and A is the mass number of the projectile. The density dependent factor is [14],

$$g(\rho) = C(1-\beta\rho^{2/3}), \quad (6)$$

with C and β taking the values 2.07 and 1.624 fm^2, respectively, obtained from nuclear matter calculation [15]. We also use an additional spin-orbit potential, $U^{\text{so}}_{n(p)}(r)$, with energy-dependent phenomenological potential depths λ_{vso} and

$\lambda_{\rm wso}$ according to the Scheerbaum prescription [16], given by

$$U^{\rm so}_{n(p)}(r) = (\lambda_{\rm vso} + i\lambda_{\rm wso})\frac{1}{r}\frac{d}{dr}\left(\frac{2}{3}\rho_{p(n)} + \frac{1}{3}\rho_{n(p)}\right), \quad (7)$$

with

$$\lambda_{\rm vso} = 130\exp(-0.013E) + 40, \quad (8)$$

$$\lambda_{\rm wso} = -0.2(E - 20). \quad (9)$$

To obtain the optical potential, the target radial matter density from the RMF calculation is folded with the NN interaction by integrating over the entire volume in coordinate space assuming spherical symmetry:

$$V_{\rm fold}(\mathbf{r},E) = \int v(|\mathbf{r} - \mathbf{r}'|,\rho,E)\rho(\mathbf{r}')d\mathbf{r}'. \quad (10)$$

Here ρ is the radial matter density of the target nucleus, which in this case is the sum of the point proton density and the point neutron density of the target from RMF calculation. The DDM3Y interaction provides only the real part of the potential. The imaginary part of the potential is taken to be identical to the real part. The final optical model potential is thus constructed by multiplying with normalization constants A_R and $A_{\rm Im}$ for real and imaginary parts, respectively as follows:

$$V_{\rm omp} = A_R V_{\rm fold} + i A_{\rm Im} V_{\rm fold}. \quad (11)$$

These normalization constants have been varied to get the best agreement with experimental cross-section values. This optical model potential has been used to study the neutron capture reaction cross sections.

DDM3Y nucleon-nucleon interaction has been used in numerous works for different perspectives, for example, to study proton radioactivity [17,18] and α-decay half-lives [19], for nuclear matter calculations [20], etc. Kobos *et al.* [12] measured differential elastic scattering cross sections for α particles on different targets. Mohr *et al.* [21] obtained the real part of the optical potential via α elastic scattering using the double-folding technique with the DDM3Y interaction for astrophysically relevant energy. The DDM3Y interaction is also used to study direct neutron capture cross sections at energies below 0.3 MeV on low-mass stable targets ^{12}C and ^{16}O [22]. We have already used it to study proton reactions at low energies [5–10]. In the present work we are applying the DDM3Y interaction in the microscopic Hauser-Feshbach statistical model prescription to check its validity at very low energies of astrophysical interest (between 1 keV and 1 MeV) for radiative neutron capture reaction cross sections on nuclei relevant to the s-process near the $N = 82$ shell-closure.

C. Cross-section calculation

The computer code TALYS-1.6 [23,24] has been used for cross-section calculations.

The statistical calculation of energy-averaged cross sections are based on the well-known Hauser-Feshbach formula given by [25]

$$\langle\sigma_{\rm re}(\alpha,\alpha')\rangle = \frac{\pi}{k_\alpha^2}\sum_{J\pi}\frac{(2J+1)}{(2I_1+1)(2I_2+1)}\frac{\left[\sum_{sl}\hat{T}_l(\alpha)\right]\left[\sum_{s'l'}\hat{T}_{l'}(\alpha')\right]}{\sum_{\alpha''s''l''}\hat{T}_{l''}(\alpha'')}. \quad (12)$$

Here, the unprimed and primed quantities represent incident and outgoing channels, respectively. The sum over α'' runs over all channels that are energetically accessible for the decay of the compound nucleus at the total energy in the incident channel. I_1 and I_2 are the spins of the target and projectile, respectively. The quantities J, π, l, and s denote total angular momentum, parity, orbital angular momentum, and spin, respectively and are determined by the usual selection rules. The transmission coefficients $\hat{T}_l(\alpha)$ of channel α for orbital angular momentum l are obtained from optical model potential constructed as described earlier. They are determined by complex phase shifts $\delta_{\alpha l}$ as

$$\hat{T}_l(\alpha) = 1 - |e^{2i\delta_{\alpha l}}|^2 \quad (13)$$

In the present case of study of (n,γ) reaction cross sections, the outgoing channel involves the emission of γ rays and hence γ-transmission coefficients are necessary, especially of dominant $E1$ transitions with appropriate giant dipole resonance energies and widths. The above equation must also be supplemented by the width fluctuation correction, especially in the case of low excitation energies, because it enhances the cross section for weak reaction channels at the cost of stronger ones. It also plays a sensitive role near the threshold of new channel openings where very different channel strengths exist. A more general discussion can be found in the manual for the TALYS-1.6 code [24].

Microscopic level densities, which are important ingredients in statistical model calculations of reaction cross sections, are taken from the calculations of Goriely *et al.* [26] included in the code. The γ-strength functions for the dominant $E1$ γ transitions are taken from Goriely's hybrid model [27]. Width fluctuation corrections in compound nuclear decay are also considered. Radial densities are taken from RMF calculations. The pairing energy correction has also been included. At low incident energies, i.e., below a few MeV, mainly binary reactions occur and very often the target and the compound nuclei only are involved in the whole reaction chain. A maximum of 30 discrete levels are taken for both target and residual nuclei. Hauser-Feshbach calculations are performed with full j,l coupling. All these options are included in the TALYS code.

III. RESULTS

A. Results of RMF calculations

The most important RMF result relevant to the calculation of neutron capture in the present formalism is the density profile. Experimental results on density are available for three nuclei with $N = 82$, viz., ^{138}Ba, ^{142}Nd, and ^{144}Sm. In Fig. 1, we plot the charge density obtained in our calculation for these three nuclei. The experimental densities for ^{138}Ba and ^{142}Nd have been generated from the parameters for a three-parameter

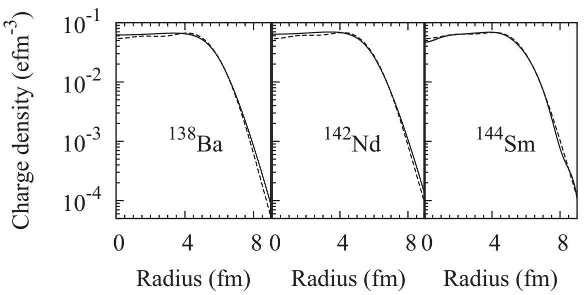

FIG. 1. Charge density in several $N = 82$ nuclei. Solid lines denote the model values using the parameters obtained from fitting the experimental data. Dashed lines indicate our results.

Gaussian function fitted to describe the electron scattering data of Heisenberg *et al.* [28]. For ^{144}Sm, the Fourier-Bessel coefficients obtained from fitting the experimental results of Moinester *et al.* [29] have been used.

Charge radius is the first moment of the charge distribution. Hence comparison between theoretical calculations and experimental data can be done to check the success of the theoretical approach. In Table II, we compare the calculated rms charge radius values with experimental data [30]. From the comparison between experimental and calculated charge density and radius values, one can infer that the present RMF calculation can describe the nuclear density near the $N = 82$ shell-closure very well. We now employ the theoretical density values to derive the optical model potential and extract cross sections for neutron capture.

TABLE II. Root-mean-square charge radii (r_c) of the nuclei studied in the present work. Experimental charge radii values are from the compilation of Angeli [30].

Nucleus	r_c(fm)		Nucleus	r_c(fm)	
	Expt.	Present		Expt.	Present
^{133}Cs	4.804	4.801	^{134}Cs	4.803	4.807
^{135}Cs	4.807	4.813	^{136}Cs	4.806	4.819
^{137}Cs	4.813	4.825			
^{130}Ba	4.829	4.797	^{132}Ba	4.831	4.808
^{134}Ba	4.830	4.820	^{135}Ba	4.827	4.826
^{136}Ba	4.833	4.832	^{137}Ba	4.833	4.837
^{138}Ba	4.838	4.843			
^{138}La	4.846	4.856	^{139}La	4.855	4.862
^{136}Ce	4.874	4.858	^{138}Ce	4.873	4.869
^{140}Ce	4.877	4.879	^{141}Ce		4.892
^{142}Ce	4.906	4.905			
^{141}Pr	4.892	4.898	^{142}Pr		4.910
^{143}Pr		4.922			
^{142}Nd	4.912	4.915	^{143}Nd	4.923	4.927
^{144}Nd	4.944	4.939	^{145}Nd	4.958	4.953
^{146}Nd	4.975	4.965	^{147}Nd	4.984	4.977
^{147}Pm		4.981	^{148}Pm		4.993
^{144}Sm	4.944	4.950	^{147}Sm	4.984	4.985
^{148}Sm	5.001	4.998	^{149}Sm	5.011	5.010

B. Result of cross-section calculation

1. Elastic scattering angular distribution

We have calculated neutron differential elastic scattering cross sections for different targets near $N = 82$ at various energies. Our interest lies in the fact that a comparison with experiments would provide a better assessment of our optical model potential. The cross sections are compared in Fig. 2. The data for ^{140}Ce for four different energies are taken from Ref. [31]. For ^{141}Pr, the data for 878 keV are taken from Cox and Dowling Cox [32] and the data for 1.2 MeV are taken from Singh and Knitter [33]. Cross sections for ^{142}Nd and ^{148}Sm are from Refs. [34] and [35], respectively.

The study of scattering at low neutron energy is important because the astrophysical reactions are usually confined to low energies. The theory agrees fairly well for ^{140}Ce and ^{141}Pr isotopes. In most of the cases the theory can reproduce the scattering cross sections in the forward direction. This trend is prominent in the cases of ^{142}Nd and ^{148}Sm.

2. Neutron capture cross section

TALYS-1.6 is meant for analysis of data above the resolved resonance range, which is approximately 1 keV. We have compared the neutron capture cross sections with those experimental measurements that do not show resolved resonances at low energy.

Theoretical neutron capture cross-section results for different neutron energy values have been compared with experimental results in Figs. 3–6. In general, we have considered the more recent results. Our main interest lies in the nuclei that are important for astrophysical *s*- and *p*-processes. We generally present only those results where a reasonable amount of experimental data exists for comparison. The exceptions are ^{139}La and ^{140}Ce because these two nuclei correspond to the $N = 82$ shell-closure.

For convenience, we present the results for the elements where only one isotope has been studied in Fig. 3. These include ^{133}Cs, ^{139}La, ^{140}Ce, and ^{141}Pr. Experimental cross-section values for the ^{133}Cs(n,γ) reaction are from Refs. [36–38]. The cross-section values are averaged over the neutron energy range because the resonances are unresolved. For example, Yamamuro *et al.* [37] used the neutron beam from a tantalum photoneutron source. They then averaged the cross sections over the appropriate energy interval. For ^{139}La, the data are from Refs. [38,39]. Similarly, here also the neutron energy has a 5% error and we get an average value for various energies. Harnood *et al.* [40] measured the neutron capture cross sections of ^{140}Ce and ^{141}Pr using the neutron TOF technique. Voss *et al.* [41] also measured the cross section for ^{141}Pr in the range 3 to 225 keV. They also calculated the MACS values from their results. Voignier *et al.* [38] also measured the capture cross section for ^{141}Pr in the energy range 0.5 to 3 MeV.

In Fig. 4, we show the average neutron capture cross sections in $^{135-138}$Ba nuclei and compare with experimental values between 1 keV and 1 MeV. Experimental cross-section values are from Refs. [42–45]. Voss *et al.* [42,43] studied the neutron capture cross sections for $^{134-137}$Ba nuclei in the energy range from 3 to 225 keV using gold as a standard.

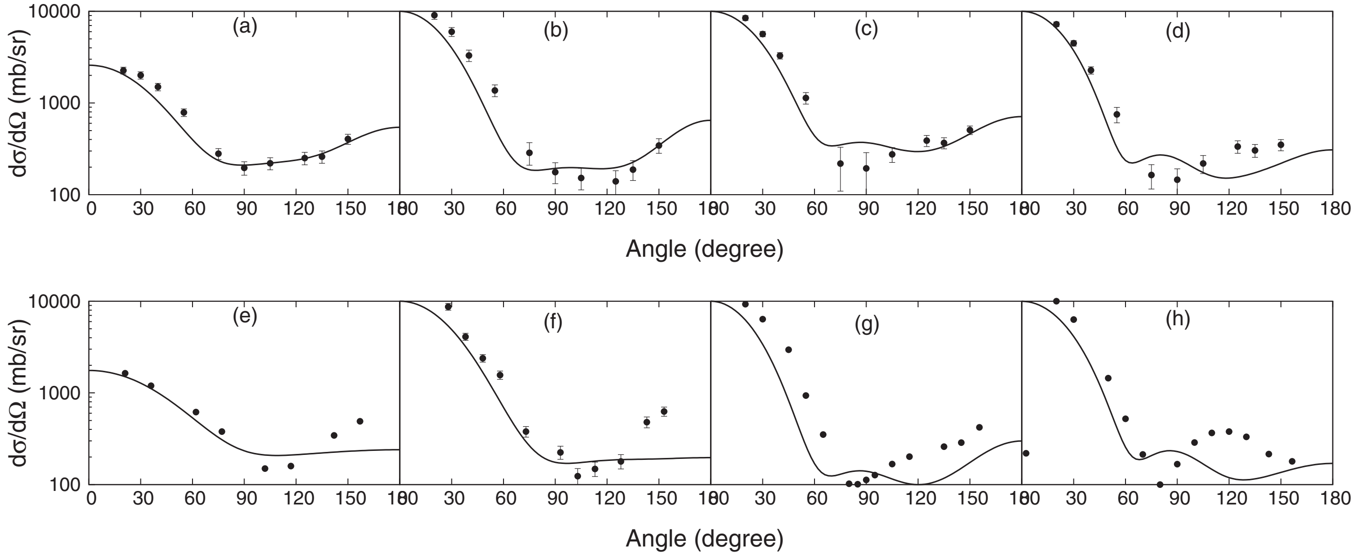

FIG. 2. Differential angular distribution for elastic scattering of neutrons from (a) ^{140}Ce at 1.5 MeV, (b) ^{140}Ce at 2.0 MeV, (c) ^{140}Ce at 2.5 MeV, (d) ^{140}Ce at 3.0 MeV, (e) ^{141}Pr at 0.878 MeV, (f) ^{141}Pr at 1.2 MeV, (g) ^{142}Nd at 2.5 MeV, and (h) ^{148}Sm at 2.47 MeV. Solid lines denote theoretical data and discrete points represent experimental data.

Neutron capture by the neutron closed shell nucleus ^{138}Ba has been studied in Refs. [44,45].

Results for neutron capture cross sections of $^{142-146}$Nd are shown in Fig. 5. Wisshak *et al.* [46,47] studied the resonances above 3 keV in $^{142-146,148}$Nd. The data were then compressed in coarse bins to get the average behavior. In another work, Veerapaspong *et al.* [48] studied the neutron capture cross sections for ^{143,145,146}Nd. Their data were put in a large energy bin of 10 keV width. Their results agree with those of Refs. [46,47] and our results, though we have not shown the data in the figure.

In Fig. 6, we plot the experimental and calculated values for $^{144,147-149}$Sm. For ^{144}Sm, experimental values are from Macklin *et al.* [49], where the authors have made measurements from 0.5 eV to 500 keV and have obtained the resonance parameters up to 100 keV. Wisshak *et al.* [50] studied the neutron capture cross section of $^{147-150,152}$Sm in the energy range 3 to 225 keV using gold as a standard. Mizumoto [51] measured the neutron capture cross sections of ^{147,149}Sm in the energy range 3 to 300 keV using the TOF technique. Diamet *et al.* [52] used a similar technique to study $^{147-150,152,154}$Sm in the energy range 10 to 90 keV.

From Figs. 3– 6, one can see that the theoretical calculations reproduce the experimental values in most of the cases. We also repeated the calculation for all the nuclei with the Jeukenne-Lejeune-Mahaux (JLM) interaction [53] to test the sensitivity of our approach. JLM is a semimicroscopic optical model potential derived from the Brückener-Hartree-Fock approximation based on Reid's hard core nucleon-nucleon interaction. We observe that our model reproduces the experimental values better than the JLM model in all the cases. As an example,

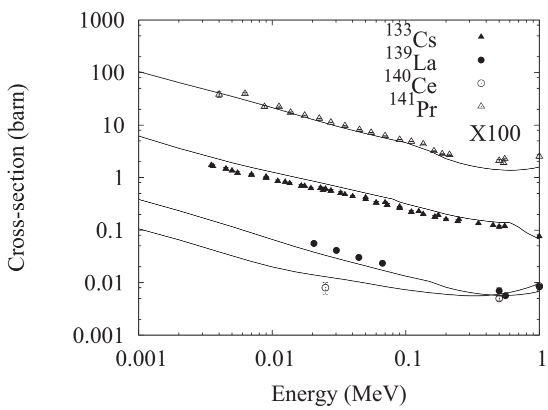

FIG. 3. Comparison of the results of the present calculation with experimental measurements for ^{133}Cs, ^{139}La, ^{140}Ce, and ^{141}Pr. The solid lines indicate the theoretical results. For convenience, cross-section values for ^{141}Pr have been multiplied by a factor of 100.

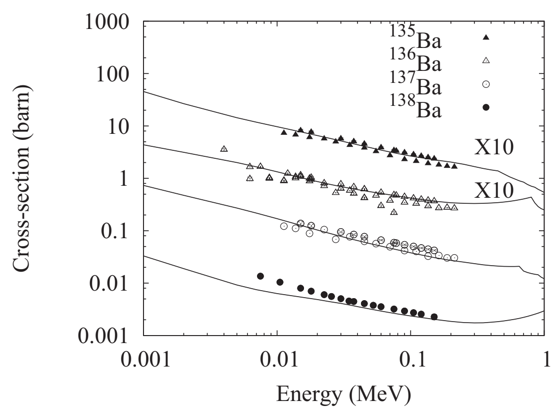

FIG. 4. Comparison of the results of the present calculation with experimental measurements for $^{135-138}$Ba. The solid lines indicate the theoretical results. For convenience, cross-section values for ^{135,136}Ba have been multiplied by a factor of 10.

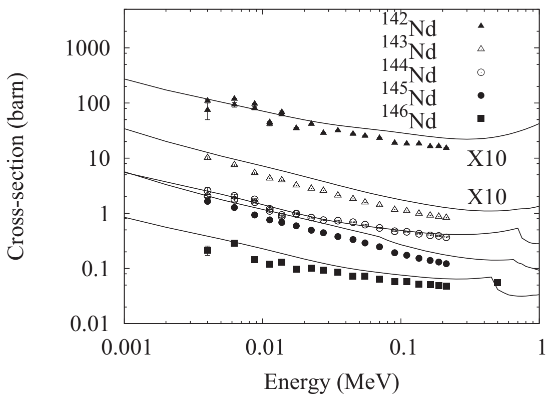

FIG. 5. Comparison of the results of the present calculation with experimental measurements for $^{142-146}$Nd. The solid lines indicate the theoretical results. For convenience, cross-section values for ^{143,144}Nd have been multiplied by a factor of 10.

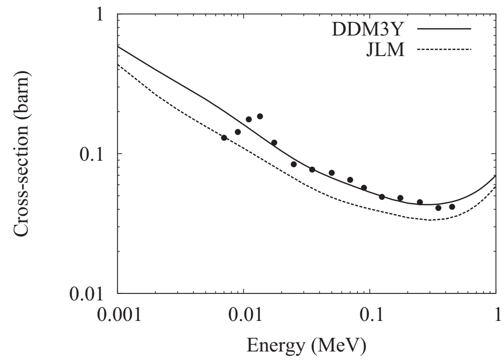

FIG. 7. The Neutron capture cross sections on the ^{144}Sm target are shown with two different optical model potential calculations and plotted against experimental data. The solid line denotes the present formalism and the dotted line represents the JLM optical model potential.

in Fig. 7 we have shown the results for ^{144}Sm. As can be easily seen, the JLM model differs from our measurement as well as from experimental data by a factor of order ∼2. For other nuclei, the trend is more or less similar. As already mentioned, we have also varied the normalization constants, particularly the imaginary part. However, we found very small changes in cross sections while varying the imaginary depth by a factor of ∼2. Hence we kept it at the value unity. In the next subsection, we employ our method to calculate the MACS for some astrophysically important nuclei.

C. Maxwellian-averaged cross sections

Apart from the nuclei with $N = 82$ in the s-process path, i.e., ^{138}Ba, ^{139}La, ^{140}Ce, ^{141}Pr, and ^{142}Nd, which act as bottlenecks due to low cross sections, neutron capture reactions in some other nuclei in the neighborhood are also important for nucleosynthesis. In Fig. 8, we show the s-process path in the neighborhood of the shell closure at $N = 82$. The shaded rectangles indicate stable and extremely long-lived nuclei. The weak branch points are indicated by rectangles with dashed lines. Similarly, weak s-process paths are indicated by dashed lines. One can see that there are strong branch points in the s-process path at ^{134}Cs, ^{147}Nd, and ^{147,148}Pm. Besides, there are weaker branch points at ^{136}Cs, ^{141}Ce, and ^{147,149}Pm. As already pointed out, the nuclei ^{134,136}Ba, ^{142}Nd, and ^{148,150}Sm are s-only. There are several p nuclei such as ^{130}Ba (not shown in Fig. 8) ^{132}Ba, ^{138}La, ^{136,138}Ce, and ^{144}Sm, the last corresponding to the shell closure.

In Table III, we present the theoretically calculated MACS values at $kT = 30$ keV for a number of selected isotopes and compare with experimental measurements whenever available. Experimental values are from the KADONIS database [54], which is an updated version of the compilation of Bao *et al.* [55]. Theoretical values from MOST calculations [56], which are listed in the KADONIS online database, are also presented. MOST is a Hauser-Feshbach code that derives all nuclear inputs from global microscopic models. As one can see, agreement of our results with experiment is better than the MOST results in almost all cases. In the next part of the discussion, we comment only on the more significant results.

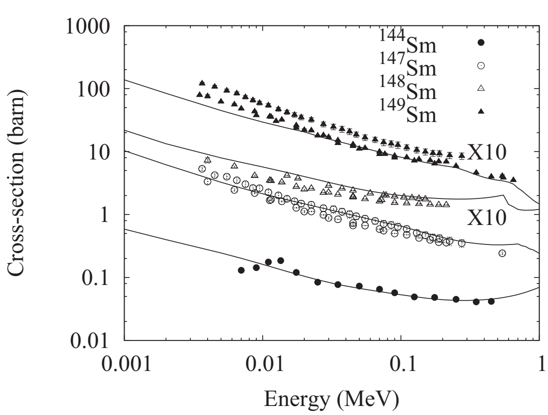

FIG. 6. Comparison of the results of the present calculation with experimental measurements for $^{144,147-149}$Sm. The solid lines indicate the theoretical results. For convenience, cross-section values for ^{148,149}Sm have been multiplied by a factor of 10.

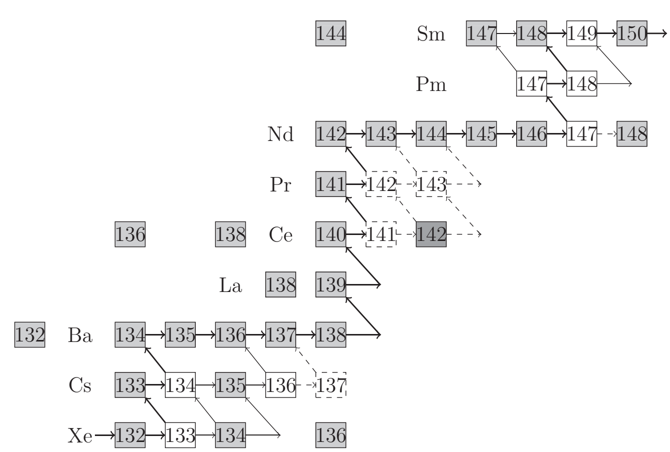

FIG. 8. The s-process path near the shell closure at $N = 82$. Also shown are some of the p nuclei. See text for more details.

TABLE III. Maxwellian-averaged cross sections at $kT = 30$ keV for nuclei near the $N = 82$ shell-closure. Experimental values are from Ref. [54]. See text for other experimental values. The nuclei with $N = 82$ are in bold font.

Nucleus	MACS (mb)			Nucleus	MACS (mb)		
	Present	Expt.	MOST		Present	Expt.	MOST
$^{133}_{55}$Cs	685	509 ± 21	469	$^{134}_{55}$Cs	786		805
$^{135}_{55}$Cs	147	160 ± 10	148	$^{136}_{55}$Cs	90.4		
$^{137}_{55}$**Cs**	16.1						
$^{130}_{56}$Ba	625.2	746 ± 34	490	$^{132}_{56}$Ba	393	397 ± 16	227
$^{134}_{56}$Ba	158	176.0 ± 5.6	117	$^{135}_{56}$Ba	528	455 ± 15	259
$^{136}_{56}$Ba	74.6	61.2 ± 2.0	49.4	$^{137}_{56}$Ba	81.8	76.3 ± 2.4	95.4
$^{138}_{56}$**Ba**	4.14	4.00 ± 0.20	2.79				
$^{138}_{57}$La	417		337	$^{139}_{57}$**La**	31.0	32.4 ± 3.1	45.9
$^{136}_{58}$Ce	547	328 ± 21	206	$^{138}_{58}$Ce	137	179 ± 5	60.5
$^{140}_{58}$**Ce**	12.7	11.0 ± 0.4	6.71	$^{141}_{58}$Ce	198.8		58.4
$^{142}_{58}$Ce	33.5	28 ± 1	16.7				
$^{141}_{59}$**Pr**	101	111.4 ± 1.4	130	$^{142}_{59}$Pr	233		261
$^{143}_{59}$Pr	170		57.7				
$^{142}_{60}$**Nd**	54.5	35.0 ± 0.7	22.9	$^{143}_{60}$Nd	362.4	245 ± 3	105
$^{144}_{60}$Nd	82.3	81.3 ± 1.5	37.1	$^{145}_{60}$Nd	617.9	425 ± 5	207
$^{146}_{60}$Nd	128.7	91.2 ± 1.0	56.8	$^{147}_{60}$Nd	1434.4		663
$^{147}_{61}$Pm	1210.4	709 ± 100	452	$^{148}_{61}$Pm	1529.7		
$^{144}_{62}$**Sm**	91.0	92 ± 6	38.6	$^{147}_{62}$Sm	1229	973 ± 10	584
$^{148}_{62}$Sm	340	241 ± 2	130	$^{149}_{62}$Sm	1622	1820 ± 17	1274

The Cs isotopes that are involved in the s-process are ^{133,134,135}Cs. The nucleus ^{134}Cs is unstable with a half-life of 2.06 yr and no neutron capture data are yet available. However, this is important for the abundances of ^{134,136}Ba in view of the strong branching at ^{134}Cs. The compilation by Bao *et al.* [55] recommended a MACS value of 664 ± 174 mb. Our calculated value for ^{135}Cs is close to the experimental measurements. However, the neutron-deficient ^{133}Cs rate is comparatively poorly reproduced.

Dillmann *et al.* [3] have measured the MACS values for a number of nuclei relevant to the p-process. The measured values at $kT = 25$ keV for the nuclei ^{130,132}Ba are 736 ± 29 mb and 392.6 ± 14.8 mb, respectively. Our calculated values for ^{130,132}Ba at 25 keV are 675.3 mb and 424.1 mb, respectively. The neutron capture cross sections of the s-only nuclei ^{134,136}Ba are very important for constraining the s-process. The cross section for ^{136}Ba is also known to be an important ingredient in determining the mean neutron exposure in the main s-process component. As one can see, here also our results are reasonably close to experimental measurements except in the case of ^{130}Ba.

Käppeler *et al.* [57] measured the cross sections for stable Ce isotopes. They then constructed an optical model potential for this region and calculated the cross sections for ^{141}La and ^{142,143}Pr in the Hauser-Feshbach formalism. Their calculated values for these two nuclei at 30 keV are 91 mb, 297 mb, and 205 mb, respectively. Although their results for ^{140,142}Ce and ^{141}Pr are very close to our calculations, the value for ^{141}Ce is smaller by more than a factor of 2, while the values for ^{142,143}Pr are larger by more than 25% and 20%, respectively. The results for La and Pr isotopes are also close to experimental measurements. The nucleus ^{138}La is produced in the p-process. However, results for more neutron-deficient Ce isotopes do not agree well with experiments.

As one goes to heavier isotopes, agreements become poorer except in a few cases such as ^{144}Nd and ^{144}Sm, though they are still better than the MOST calculations. In general, the poor agreements may be due to the fact that, away from the closed shell, deformation effects come into the picture. However, our calculation is unable to explain the recent results for ^{142}Nd, a spherical nucleus with $N = 82$, though some of the older measurements for ^{142}Nd are closer to our calculation. Results for all the other nuclei with $N = 82$ are explained with a good accuracy.

The differences between our calculations and the MOST data can be attributed to the different choice of nucleon-nucleon interactions as well as different choices for certain inputs, especially, nuclear level densities and $E1$ γ-ray strength function. The MOST calculation is based on the JLMB nucleon potential [58], a revised version of the JLM potential introduced by Jeukenne *et al.* [53]. A large contribution to uncertainty in nuclear rate calculation comes from the ambiguity in the

TABLE IV. Maxwellian-averaged neutron capture cross sections of ^{138}Ba, ^{139}La, ^{140}Ce, ^{141}Pr, and ^{142}Nd. The experimental values presented are from Ref. [54]. See text for more details about the experiments and the available latest measurements not included in Ref. [54].

kT (MeV)	MACS (mb)									
	^{138}Ba		^{139}La		^{140}Ce		^{141}Pr		^{142}Nd	
	Present	Expt.	Present	Expt.	Present	Expt.	Present	Expt.	Present	Expt.
0.005	10.3	13.4	118	111.2	34.0	23	353	412	146.5	98.6
0.010	6.96	7.85	68.9	63.2	21.9	19.5	215	247	95.8	65.1
0.015	5.68	5.93	50.8	48.1	17.6	16	161	182	76.2	51.3
0.020	4.93	4.95	41.2	40.3	15.2	13.5	132	148	65.8	43.4
0.025	4.46	4.38	35.2	35.7	13.8	12	114	126	58.8	38.4
0.030	4.14	4.00	31.0	32.4	12.7	11.0	101	111	54.5	35.0
0.040	3.61	3.49	25.4	27.7	11.2	9.5	82.8	91.5	47.9	30.7
0.050	3.28	3.14	21.8	23.6	10.2	8.7	70.8	78.3	43.8	27.7
0.060	3.08	2.89	19.2	22.0	9.5	8.1	62.0	69.0	41.0	25.5
0.080	2.76	2.52	15.8	18.4	8.6	7.2	50.1	56.2	37.4	22.9
0.100	2.58	2.23	13.7	15.2	8.0	6.6	42.4	47.6	35.5	21.0

nuclear level density. MOST uses microscopic Hartree-Fock-BCS level densities from Ref. [59] that are treated with shell and pairing effects, deformation, and collective excitation. However we have taken the level density from Ref. [26], which is based on a microscopic combinational model explicitly taking into account the vibrational contribution of phonon excitations along with the rotational enhancement factor. This model is also coupled with suitable renormalization factors to reproduce experimental s- and p-wave neutron resonance spacings with a moderate degree of accuracy and thus reliable extrapolation at low energies is possible. The other significant input that differs from our calculation is $E1$ γ-ray strength that has been taken from quasi-particle-random-phase approximation (QRPA) calculation [60] in the case of MOST calculation and from Ref. [27] in the present method.

As already pointed out, modern measurements have emphasized the importance of the MACS values at various thermal energies. Hence a number of works, apart from those already mentioned, have measured the MACS values at different temperatures. We present the MACS values at different temperatures for $N = 82$ isotopes in Table IV and draw attention to some important results. Heil *et al.* [61] have used neutron activation studies to measure the MACS value at 5.1 keV as 13.0 ± 0.5 mb in ^{138}Ba. In the present work, the MACS value for ^{138}Ba is calculated to be 10.2 mb at $kT = 5.1$ keV.

Natural lanthanum is nearly monoisotopic. It is an important element as it can be easily detected in solar spectroscopy. It is produced in both s- and r-processes and is particularly suitable for monitoring s-process abundances from Ba to Pb. This has led to the study of ^{139}La through neutron TOF spectroscopy as well as activation measurement. In Table IV, we present the MACS values for this isotope at different temperatures. O'Brien *et al.* [62] have measured the MACS values at $kT = 30$ keV as 31.6 ± 0.6 mb. Our calculated value of 31.0 mb agrees with the measurements. The activation technique has also been used to measure MACS at $kT = 5$ keV. The measured value 113.7 ± 4.0 mb [63] is in excellent agreement with our calculation. Terlizzi *et al.* have measured the resonance parameters in the energy range 0.6 to 9 eV and have recalculated the MACS values in the light of their measurements [64]. Their values also lie close to our calculated results. For example, their measurement yields a value of 106.9 ± 5.3 mb at $kT = 5$ keV after normalization to the value for 25 keV from Ref. [62].

Käppeler *et al.* [57] also used the ^{7}Li$(p,n)^7$Be reaction to study the thermal neutron capture by Ce isotopes at 25 keV. They obtained a MACS value of 12.0 ± 0.4 mb. This was extrapolated to other thermal energy values. As already mentioned, Voss *et al.* [41] have obtained the MACS values as a function of temperature for ^{141}Pr.

As already mentioned, Wisshak *et al.* [46] studied the neutron capture cross sections of Nd isotopes. They have also calculated the MACS values at different energies from their data. Guber *et al.* [65] also measured the MACS values between $kT = 5$ and 50 keV. Both the above references have commented on the importance of the new measurements in the s-process.

IV. SUMMARY

To summarize, astrophysically important neutron capture reactions near the $N = 82$ shell-closure have been studied using a microscopic approach. Densities of relevant nuclei have been calculated in the RMF approach. The calculated charge densities and radii agree with experimental measurements, whenever available. The calculated density has been folded with the DDM3Y nucleon-nucleon interaction to obtain the optical model potential for neutron reactions. Cross sections for (n,γ) reactions have been calculated and compared with measurements. Finally MACS values, important for s- and p-processes, have been calculated.

ACKNOWLEDGMENTS

The authors acknowledge the financial support provided by the University Grants Commission (JRF and DRS), Department of Science and Technology, the Alexander Von Humboldt Foundation, and the University of Calcutta.

[1] M. E. Burbidge, G. R. Burbidge, W. A. Fowler, and F. Hoyle, Rev. Mod. Phys. **29**, 547 (1957).
[2] F. Käppeler, R. Gallino, S. Bisterzo, and W. Aoki, Rev. Mod. Phys. **83**, 157 (2011).
[3] I. Dillmann, C. Domingo-Pardo, M. Heil, F. Käppeler, S. Walter, S. Dababneh, T. Rauscher, and F.-K. Thielemann, Phys. Rev. C **81**, 015801 (2010).
[4] B. G. Todd-Rutel and J. Piekarewicz, Phys. Rev. Lett. **95**, 122501 (2005).
[5] G. Gangopadhyay, Phys. Rev. C **82**, 027603 (2010).
[6] C. Lahiri and G. Gangopadhyay, Eur. Phys. J. A **47**, 87 (2011).
[7] C. Lahiri and G. Gangopadhyay, Phys. Rev. C **84**, 057601 (2011).
[8] C. Lahiri and G. Gangopadhyay, Phys. Rev. C **86**, 047601 (2012).
[9] S. Dutta, D. Chakraborty, G. Gangopadhyay, and A. Bhattacharyya, Phys. Rev. C **91**, 025804 (2015).
[10] D. Chakraborty, S. Dutta, G. Gangopadhyay, and A. Bhattacharyya, Phys. Rev. C **91**, 057602 (2015).
[11] A. Bouyssy, J. F. Mathiot, N. Van Giai, and S. Marcos, Phys. Rev. C **36**, 380 (1987).
[12] A. M. Kobos, B. A. Brown, P. E. Hodgson, G. R. Satchler, and A. Budzanowski, Nucl. Phys. A **384**, 65 (1982).
[13] G. R. Satchler and W. G. Love, Phys. Rep. **55**, 183 (1979).
[14] W. D. Myers, Nucl. Phys. A **204**, 465 (1973).
[15] D. N. Basu, J. Phys. G: Nucl. Part. Phys. **30**, B7 (2004).
[16] R. R. Scheerbaum, Nucl. Phys. A **257**, 77 (1976).
[17] M. Bhattacharya and G. Gangopadhyay, Phys. Lett. B **651**, 263 (2007).
[18] D. N. Basu, P. R. Chowdhury, and C. Samanta, Phys. Rev. C **72**, 051601 (2005).
[19] P. R. Chowdhury, C. Samanta, and D. N. Basu, Phys. Rev. C **73**, 014612 (2006).
[20] D. T. Khoa and W. von Oertzen, Phys. Lett. B **304**, 8 (1993).
[21] P. Mohr, T. Rauscher, H. Oberhummer, Z. Máté, Zs. Fülöp, E. Somorjai, M. Jaeger, and G. Staudt, Phys. Rev. C **55**, 1523 (1997).
[22] H. Kitazawa, M. Igashira, T. Ohsaki, and T. Matsushima, J. Nucl. Sci. Technol. **39**, 799 (2002).
[23] A. J. Koning, S. Hilaire, and M. Duizvestijn, in *Proceedings of the International Conference on Nuclear Data for Science and Technology, April 22–27, 2007, Nice, France*, edited by O. Bersillon, F. Gunsing, E. Bauge, R. Jacqmin, and S. Leray (EDP Sciences, Les Ulis, Paris, France, 2008), p. 211.
[24] http://www.talys.eu.
[25] See, for example, C. Iliadis, *Nuclear Physics of Stars* (Wiley-VCH Verlag GmbH & Co., Boschstr., Weinheim, Germany, 2007).
[26] S. Goriely, S. Hilaire, and A. J. Koning, Phys. Rev. C **78**, 064307 (2008).
[27] S. Goriely, Phys. Lett. B **436**, 10 (1998).
[28] J. Heisenberg, R. Hofstadter, J. S. McCarthy, I. Sick, M. R. Yearian, B. C. Clark, R. Herman, and D. G. Ravenhall, in *Topics in Modern Physics: Tribute to E. U. Condon*, edited by W. E. Brittin and H. Odabasi (Hilger, London, 1970), p. 169.
[29] M. A. Moinester, J. Alster, G. Azuelos, J. B. Bellicard, B. Frois, M. Huet, P. Leconte, and P. X. Ho, Phys. Rev. C **24**, 80 (1981).
[30] I. Angeli, At. Data Nucl. Data Tables **87**, 185 (2004).
[31] I. A. Korzh, V. A. Mishchenko, V. D. Ovdienko, M. V. Pasechnik, and N. M. Pravdivy, Ukr. Fiz. Zh. **34**, 1173 (1989).
[32] S. A. Cox and E. E. Dowling Cox, Argonne National Laboratory Report Series, 7935 (1972).
[33] R. Singh and H. H. Knitter, Z. Phys. A **272**, 47 (1975).
[34] D. F. Coope, S. N. Tripathi, M. C. Schell, and M. T. McEllistrem, Bull. Am. Phys. Soc. **24**, 854 (GC10) (1979).
[35] D. F. Coope, S. N. Tripathi, M. C. Schell, J. L. Weil, and M. T. McEllistrem, Phys. Rev. C **16**, 2223 (1977).
[36] R. L. Macklin, J. Nucl. Sci. Eng. **81**, 418 (1982).
[37] N. Yamamuro, M. Igashira, T. Sekiya, and H. Shirayanagi, J. Nucl. Sci. Technol. (Tokyo) **20**, 797 (1983).
[38] J. Voignier, S. Joly, and G. Grenier, Nucl. Sci. Eng. **112**, 87 (1992).
[39] M. Igashira, M. Saito, J. Nishiyama, T. Ohsaki, and T. Katabuchi, Proc. Intern. Conf. Nucl. Data Sci. Technol. **2**, 1299 (2007); *Proceedings of the International Conference on Nuclear Data for Science and Technology, Nice, France, April 22–27, 2007*, edited by O. Bersillon, F. Gunsing, E. Bauge, R. Jacqmin, and S. Leray (EDP Sciences, 2008), p. 1299.
[40] S. Harnood, M. Igashira, T. Matsumoto, S. Mizuno, and T. Ohsaki, J. Nucl. Sci. Technol. (Tokyo) **37**, 740 (2000).
[41] F. Voss, K. Wisshak, C. Arlandini, F. Käppeler, L. Kazakov, and T. Rauscher, Phys. Rev. C **59**, 1154 (1999).
[42] F. Voss, K. Wisshak, K. Guber, F. Käppeler, and G. Reffo, Phys. Rev. C **50**, 2582 (1994).
[43] F. Voss, K. Wisshak, and F. Käppeler, Phys. Rev. C **52**, 1102 (1995).
[44] H. Beer, F. Corvi, and P. Mutti, Astron. J. **474**, 843 (1997).
[45] H. Beer and F. Käppeler, Phys. Rev. C **21**, 534 (1980).
[46] K. Wisshak, F. Voss, F. Käppeler, L. Kazakov, and G. Reffo, Phys. Rev. C **57**, 391 (1998).
[47] K. Wisshak, F. Voss, and F. Käppeler, Phys. Rev. C **57**, 3452 (1998).
[48] T. Veerapaspong, M. Igashira, S. Mizuno, J. Hori, and T. Ohsaki, J. Nucl. Sci. Technol. (Tokyo) **36**, 855 (1999).
[49] R. L. Macklin, N. W. Hill, J. A. Harvey, and G. L. Tweed, Phys. Rev. C **48**, 1120 (1993).
[50] K. Wisshak, K. Guber, F. Voss, F. Käppeler, and G. Reffo, Phys. Rev. C **48**, 1401 (1993).
[51] M. Mizumoto, Nucl. Phys. A **357**, 90 (1981).
[52] B. Diamet. M. Igashira, M. Mizumachi, S. Miziuno, J. Hori, K. Masuda, and T. Ohsaki, J. Nucl. Sci. Technol. (Tokyo) **36**, 865 (1999).
[53] J. P. Jeukenne, A. Lejeune, and C. Mahaux, Phys. Rev. C **16**, 80 (1977).
[54] I. Dillmann, R. Plag, F. Käppeler, and T. Rauscher, KADoNiS v0.3—The third update of the "Karlsruhe Astrophysical Database of Nucleosynthesis in Stars," in *EFNUDAT Fast Neutrons, Proceedings of the Scientific Workshop on Neutron Measurements, Theory and Applications, 28–30 April, 2009, Geel, Belgium*, edited by F.-J. Hambsch (Publications Office of the European Union, Luxembourg, 2010), p. 55; http://kadonis.org.
[55] Z. Y. Bao, H. Beer, Käppeler, F. Voss, and K. Wisshak, At. Data Nucl. Data Tables **76**, 70 (2000).
[56] M. Arnould and S. Goriely, Phys. Rep. **384**, 1 (2003).
[57] F. Käppeler, K. A. Toukan, M. Schumann, and A. Mengoni, Phys. Rev. C **53**, 1397 (1996).

[58] E. Bauge, J. P. Delaroche, and M. Girod, Phys. Rev. C **63**, 024607 (2001).
[59] P. Demetriou and S. Goriely, Nucl. Phys. A **695**, 95 (2001).
[60] S. Goriely and E. Khan, Nucl. Phys. A **706**, 217 (2002).
[61] M. Heil, S. Dababneh, A. Juseviciute, F. Käppeler, R. Plag, R. Reifarth, and S. O'Brien, Phys. Rev. C **71**, 025803 (2005).
[62] S. O'Brien, S. Dababneh, M. Heil, F. Käppeler, R. Plag, R. Reifarth, R. Gallino, and M. Pignatari, Phys. Rev. C **68**, 035801 (2003).
[63] N. Winckler, S. Dababneh, M. Heil, F. Käppeler, R. Gallino, and M. Pignatari, Astron. J. **647**, 685 (2006).
[64] R. Terlizzi *et al.*, Phys. Rev. C **75**, 035807 (2007).
[65] K. H. Guber, R. R. Spencer, P. E. Koehler, and R. R. Winters, Phys. Rev. Lett. **78**, 2704 (1997).